Effects of Nanoparticle Treatment on the Crystallization Behavior and Mechanical Properties of Polypropylene/ Calcium Carbonate Nanocomposites

Weitao Wan,[1,2] Demei Yu,[1,2] Yunchuan Xie,[1,2] Xiusheng Guo,[1,2] Wandi Zhou,[1] Jiping Cao[3]

[1]*Department of Applied Chemistry, Xi'an Jiaotong University, Xi'an 710049, People's Republic of China*
[2]*State Key Laboratory of Electrical Insulation and Power Equipment, Xi'an Jiaotong University, Xi'an 710049, People's Republic of China*
[3]*Research Institute of Modern Chemistry, Xi'an 710065, People's Republic of China*

Received 2 March 2005; accepted 1 April 2006
DOI 10.1002/app.24561
Published online in Wiley InterScience (www.interscience.wiley.com).

ABSTRACT: Effects of nanoparticle surface treatment on the crystallization behavior and mechanical properties of polypropylene (PP)/$CaCO_3$ nanocomposites were investigated by using differential scanning calorimetry (DSC), polarized optical microscope (POM), X-ray diffraction (XRD), transmission electron microscopy (TEM), and scanning electron microscopy (SEM). The results demonstrated that the interfacial interaction formed between PP and nanoparticles significantly influenced the thermal and mechanical properties of nanocomposites. It was found that $CaCO_3$ nanoparticles modified by a single aluminate coupling agent (CA-1) could improve the onset crystallization temperature more effectively than that modified by a compound surface-treating agent (CA-2) could. However, there is no significant difference in total rate of crystallization for the two PP/$CaCO_3$ nanocomposites (PPC-1 and PPC-2), which contained CA-1 and CA-2, respectively. In contrast, CA-2 modified nanoparticles could cause smaller spherulites and induce much more β-phase crystal in nanocomposites than that of CA-1 modified nanoparticles. This may be explained by a synergistic effect of aluminate coupling agent and stearic acid in CA-2, which also resulted in an improved toughness for PPC-2. © 2006 Wiley Periodicals, Inc. J Appl Polym Sci 102: 3480–3488, 2006

Key words: nanocomposites; poly(propylene); surface modification; crystallization; synergistic effect

INTRODUCTION

Polypropylene (PP) (which has relative high thermal stability, good mechanical properties, and facile processability) is one of the most widely used commercial plastics. However, its relative low service temperature and low toughness under severe conditions limits its usage. Recently, modification of Polypropylene using nanoparticles has attracted considerable interests because it can markedly enhance physical properties of PP materials.[1–17]

$CaCO_3$ nanoparticle (which can improve the toughness and the rigidity, and affect the crystallization behavior of polymer matrix, plus its low cost and wide availability) has received much research interest.[18–22] The interface between $CaCO_3$ nanoparticles and PP matrix, and the dispersing state of nanoparticles in the matrix are two key factors in achieving PP/$CaCO_3$ nanocomposites with high performance. Accordingly, it is very important to control the surface state of nanoparticles. There are some reports on the relationship between the interface and the properties of PP/$CaCO_3$ nanocomposites. For examples, Ansari and Price prepared PP/$CaCO_3$ nanocomposites by using $CaCO_3$ nanoparticle modified by sodium polyacrylate, stearic acid, or both, indicating that there were a good correlation between the physical properties and the different surface energy of the filler in PP/$CaCO_3$ composites.[23] Zhang et al. used a nonionic modifier (polyoxyethylene nonyphenol) to improve the dispersion of $CaCO_3$ nanoparticles, and found that the Izod impact energy of the composites increased significantly while the tensile properties did not change much.[24] Other results showed the effect of $CaCO_3$ nanoparticles on the crystallization behavior of composites.[25,26] For example, it was reported that the addition of acrylic acid-grafted polypropylene as compatilizer improved the nucleation of $CaCO_3$ nanoparticles in PP/$CaCO_3$ nanocomposites, and the crystallization temperature of the composites increased because of the enhanced nucleation of the nanoparticles.[27]

In this study, $CaCO_3$ nanoparticles were surface modified by a single aluminate coupling agent and a

Correspondence to: D. Yu (dmyu@mail.xjtu.edu.cn).
Contract grant sponsor: National Natural Science Foundation; contract grant number: 50177026.
Contract grant sponsor: Ministry of Education, People's Republic of China; contract grant number: [(2002) 350].
Contract grant sponsor: State Key Laboratory of Electrical Insulation and Power Equipment.

compound surface-treating agent, respectively. The investigation was focused on the different effects of the two-nanoparticle treatments on the crystallization behavior and mechanical properties of PP/$CaCO_3$ nanocomposites.

EXPERIMENTAL

Materials

Polypropylene (1001A) with density 0.91 kg/L was provided by Beijing YanShan Petrochemical Co., P. R. China. $CaCO_3$ nanoparticles with the average size of 60–80 nm were obtained from EnPing Chemical Industry, P. R. China. The aluminate coupling agent (CA-1) was provided by the Institute of Polymer Science, Fujian Normal University, P. R. China. The compound surface-treating agent (CA-2), containing CA-1 and stearic acid compatilizer, was prepared in our laboratory. The chemical structures of these materials were given in Table I.

Sample preparation

Surface modification for $CaCO_3$ nanoparticles

The $CaCO_3$ nanoparticles were surface modified by CA-1 and CA-2, respectively. The procedure of surface modification for the $CaCO_3$ nanoparticles was shown as follows. A 9 : 1 (weight) solution of ethanol and distilled water was first prepared, and then a certain amount of CA-1 (or CA-2) was added to that prepared solution and dispersed in an ultrasonic bath for 5 min for hydrolysis reaction. After that, the mixed solution was poured into the slurry of $CaCO_3$ nanoparticles and kept in an ultrasonic bath for 30 min. The resulting products were washed, filtered, and then allowed to dry at 80°C in a vacuum oven for 12 h.

Preparation of PP/$CaCO_3$ nanocomposites

Before preparation of the nanocomposites, PP and surface-treated $CaCO_3$ nanoparticles were dried in vacuum oven at 100°C for 5 h and naturally cooled down to room temperature. PP/$CaCO_3$ nanocomposites with the $CaCO_3$ nanoparticles modified by CA-1 (denoted as PPC-1) and with the $CaCO_3$ nanoparticles modified by CA-2 (denoted as PPC-2) were prepared by melt blending in a Haake mixer (Haake Rheccord 90, Germany) at 185°C and 120 rpm. The mix ended after the melt torque stabilized for 1 min. The resulting samples of pure PP and PP/$CaCO_3$ nanocomposites were hot pressed into sheets with thickness of 2 and 4 mm at 180°C for 3 min under a pressure of 15 MPa. The modified $CaCO_3$ nanoparticles loading in PPC-1 and PPC-2 were both 3.0 wt %.

Characterization of the nanocomposites

Fourier transformed infrared spectroscopy

Fourier transformed infrared (FTIR) spectra were recorded with a Nicolet AVATAR-IR 360 spectrometer (Nicolet Instrument Co., USA) by a solid potassium bromide method.

Transmission electron microscopy

The dispersion of the surface-modified $CaCO_3$ nanoparticles in PP matrix was observed by a JEOL JEM-2010 transmission electron microscope (TEM) with an accelerating voltage of 200 kV. A thin layer of about 80 nm thick from the sample was cryogenically sectioned using an Ultracuts (Leica) microtome.

Differential scanning calorimeter

Melting process of the samples, directly cut from the molded sheet, was carried out on a Netzsh DSC 200PC differential scanning calorimeter (DSC), and the temperature was calibrated with indium. The samples (5–6 mg) were heated continuously from room temperature to 180°C at the rate of 5°C/min.

For the crystallization process of nanocomposites, the same samples were first heated rapidly from room temperature to 160°C at the rate of 50°C/min and then to 170°C at the rate of 20°C/min step by step to make the samples melt completely. After that, the melted samples were kept in the aluminum cell at 170°C for 10 min to eliminate the thermal history, then the melted samples were cooled down to room temperature at the rate of 10°C/min. Finally, the samples were heated to 180°C at the rate of 10°C/min again. All measurements were carried out under the nitrogen atmosphere environment.

X-ray diffraction

The structures of pure PP and PP/$CaCO_3$ nanocomposites were determined with a Shimadzu XRD-6000

TABLE I
Chemical Structures of the Employed Materials

Materials	Chemical Structure
Aluminates coupling agent (CA-1)	$(C_3H_7O)_xAl(OCOR^1)_m(OCOR^2)_n(OAB)_y$
Stearic acid (Octadecanoic acid)	$CH_3(CH_2)_{16}COOH$
Compound surface-treating agent (CA-2)	CA-1 + Stearic acid

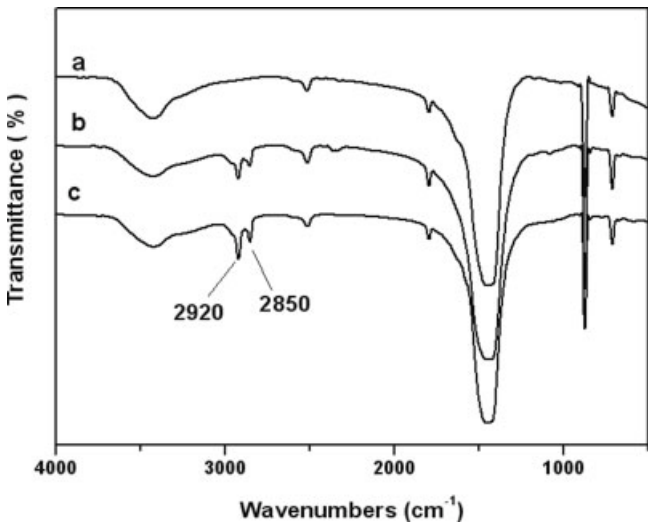

Figure 1 FTIR spectra for: (a) surface unmodified $CaCO_3$ nanoparticles; (b) CA-1 surface modified $CaCO_3$ nanoparticles; (c) CA-2 surface modified $CaCO_3$ nanoparticles.

diffractometer. The X-ray diffraction (XRD) is equipped with a graphite homochromatic instrument and a Cu anticathode (40 kV, 30 mA, scanning rate = 2°/min, 2θ = 5–40°). The experiments were conducted at ambient temperature (25°C).

Polarized optical microscope

The spherulite morphology of PP/$CaCO_3$ nanocomposite was observed with an Olympus BX51 polarized optical microscope (POM) equipped with a crossed polarizer and a hot stage (Linkam THMS600). The samples were hot pressed into films of thickness ~ 0.02 mm. After that, the film sample was heated to 180°C and kept for 3 min via the hot stage, then the sample was cooled down to room temperature at a rate of 10°C/min.

Measurement of mechanical properties

Standard specimens were sampled from the compression molded sheet and then conditioned at the temperature of (23 ± 2)°C and the relative humidity of 50 ± 5% for 40 h. Tensile test was measured according to ASTM D638 at a crosshead speed of 20 mm/min, and Izod notched impact test was assessed according to ASTM D256.

Scanning electron microscopy

The fracture morphology of PP/$CaCO_3$ nanocomposites was studied using Hitachi S-2700 scanning electron microscopy (SEM). The selected specimens were coated with a thin layer of gold prior to microscopy to avoid charge buildup.

RESULTS AND DISCUSSION

Mechanism of surface modification

Coupling agent improves the adhesion by forming a thin interfacial layer that bridges two components. The bridging effect of the interfacial layer is achieved through chemical and physical interactions among the coupling layer, nanoparticle and polymer matrix.[28] In the present study, CA-1 and CA-2 were used to establish such a coupling layer between the $CaCO_3$ nanoparticles and PP matrix.

On the basis of the molecular structure of the coupling agent, there can easily form the hydroxyl group under proper conditions by the hydrolysis reaction. The resultant hydroxyl group is hydrophilic in nature; therefore, the hydrolyzed coupling agent easily wets the nanoparticle surface. Moreover, the hydrolyzed coupling agent is able to react with the hydroxyl groups on the surface of $CaCO_3$ nanoparticles to form strong chemical bonds between the nanoparticles and coupling agent layer.

The other end of the coupling agent has a relative high miscibility with the hydrophobic PP matrix. During melt blending with the mechanical shearing force and the high temperature, strong chemical bonding and some physical force between the coupling agent layer and the PP matrix will be established.

Figure 1 shows the FT-IR spectra for surface modified (panel b, c) and surface unmodified $CaCO_3$ nanoparticles (panel a), respectively. Compared with the unmodified nanoparticles, there presents two obvious peaks at wavenumbers of 2920 and 2850 cm^{-1} for both CA-1 and CA-2 modified $CaCO_3$ nanoparticles. The two peaks are attributed to the carbon–hydrogen stretch absorption of —CH_2 groups, coming from the long aliphatic chains of the used coupling agent. Therefore, it is confirmed that there exists strong chemical bonds between the nanoparticles and coupling agents. Besides, the results also shows that the absorption intensity of —CH_2 groups for CA-2 modified $CaCO_3$ nanoparitlces is much stronger than that of CA-1 modi-

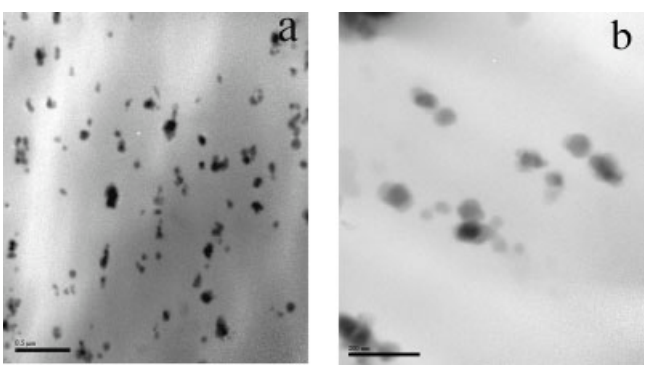

Figure 2 TEM micrograph of PP/$CaCO_3$ nanocomposites with CA-1 viewed under low (a) and high (b) magnifications.

fied $CaCO_3$ nanoparticles. This may be due to a synergistic effect existing in the compound coupling agent of CA-2, which is favorable to the chemical bonding reaction.

Dispersion of nanoparticles in PP matrix

Figure 2 and Figure 3 show the TEM micrographs of PPC-1 and PPC-2 nanocomposites, respectively. In both PPC-1 and PPC-2, most modified $CaCO_3$ nanoparticles are well dispersed in PP matrix while some nanoparticles aggregate. The individual $CaCO_3$ nanoparticles could also be observed clearly from the two magnified TEM micrographs. The average size of nanoparticles is approximate 60–80 nm. Furthermore, compared with CA-1 modified $CaCO_3$ nanoparticles in PP matrix shown in Figure 2, a relative good dispersion is achieved when the $CaCO_3$ nanoparticles were modified by CA-2 as shown in Figure 3, indicating that CA-2 could improve the compatibility of $CaCO_3$ nanoparticles with PP matrix more effectively than CA-1. This may be due to a stronger interfacial interaction achieved in PPC-2.

Crystallization and melting behavior of nanocomposites

The DSC thermograms of crystallization process for pure PP and the two PP/$CaCO_3$ nanocomposites (PPC-1 and PPC-2) at the cooling rate of 10°C/min are shown in Figure 4. It shows that the value of crystallization peak temperature (T_p) for the nanocomposites is higher than that of pure PP, and the value of T_p for PPC-1 is about 3°C higher than that of PPC-2. All the values of T_p are listed in Table II.

Obviously, the heterogeneous nucleating effect of the $CaCO_3$ nanoparticles causes the increase in crystallization temperature of nanocomposites. Since it has been reported that single stearic acid has no influence on the crystallization process of PP.[29–31] The difference

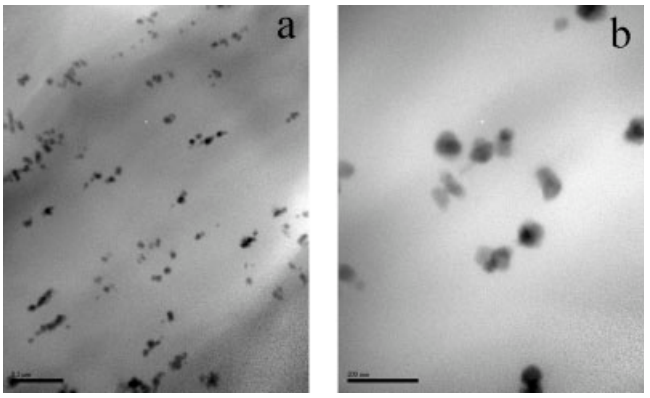

Figure 3 TEM micrograph of PP/$CaCO_3$ nanocomposites with CA-2 viewed under low (a) and high (b) magnifications.

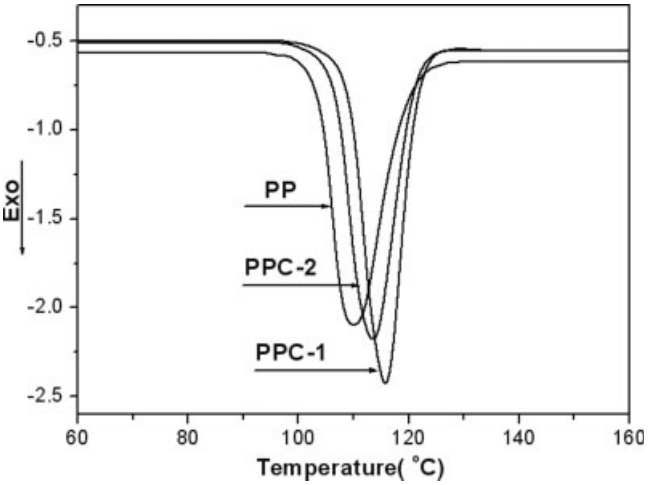

Figure 4 DSC thermogram of PP and PP/$CaCO_3$ nanocomposites at the cooling rate of 10°C/min.

in values of T_p between PPC-1 and PPC-2 may come from a synergistic effect of aluminate coupling agent and stearic acid. Usually, the crystallization of a polymer includes two processes: one is the nucleation process, and the other is the crystal growth process. Compared with CA-1, CA-2 contains the stearic acid compatilizer that could enhance the interaction between the coupling agent and the macromolecular chains of PP. Meanwhile, the enhanced interaction could restrain the motion of macromolecular chains of PP to some extent and affect the crystallization process. Therefore, it retards the crystallization and increases the inducing time of crystallization for the nanocomposites. As a result, the crystallization peak of PPC-2 appears at the lower temperature.

After the process of crystallization, the samples were reheated. The DSC heating curves of PP and PP/$CaCO_3$ nanocomposites are displayed in Figure 5. It indicates that there are nearly no changes in the shape of curves for pure PP and PP/$CaCO_3$ nanocomposites. Both pure PP and PP/$CaCO_3$ nanocomposites seem to have the same value of melting temperature T_m (The peak temperature of heating curve describes the melting temperature). These values are listed in Table II. On the basis of the area of heating curves in Figure 5, the degrees of crystallinity X_c for pure PP and PP/

TABLE II
Values of T_p, ΔH_f, T_m, and X_c of PP and PP/$CaCO_3$ Nanocomposites

Sample	T_p (°C)	ΔH (J/g)	T_m (°C)	X_c (%)
PP	110.1	85.3	167.3	40.8
PPC-1	116.0	89.0	166.9	42.6
PPC-2	113.5	88.0	167.3	42.1

T_p: crystallization peak temperature; ΔH: heat of fusion; T_m: melting temperature; X_c: degree of crystallinity.

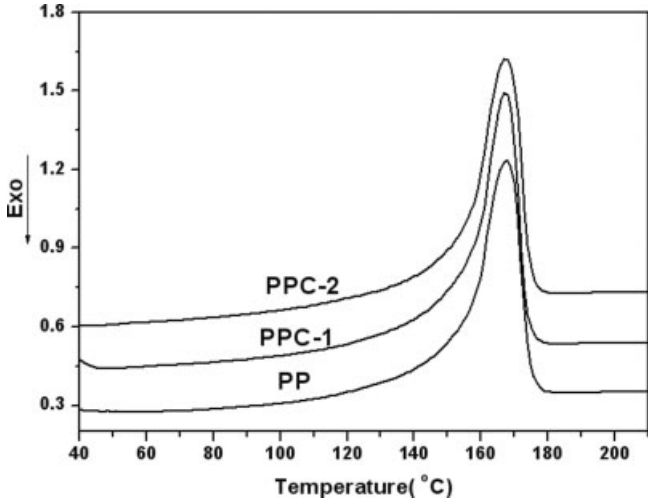

Figure 5 DSC heating curves of PP and PP/$CaCO_3$ nanocomposites after crystallization at the cooling rate of 10°C/min.

$CaCO_3$ nanocomposites can be calculated by the following equation[32]

$$X_c = \frac{\Delta H}{(1-\varphi)\Delta H_0} \times 100\%$$

where ΔH is the endothermal enthalpy of the sample, ΔH_0 is the endothermal enthalpy of PP when it crystallizes completely, and the value is set as 209.0 J/g according to the database of DSC apparatus. φ is the mass fraction of the filler. Values of X_c for PP and nanocomposites are also listed in Table II. The degree of crystallinity for PP/$CaCO_3$ nanocomposites is higher than that of pure PP. However, there is no obvious difference in the degrees of crystallinity between PPC-1 and PPC-2.

TABLE III
Parameters of Crystallization Kinetics for PP and PP/$CaCO_3$ Nanocomposites at the Cooling Rate of 10°C/min

Sample	n	Z_c	$t_{1/2}$ (min)
PP	2.82	0.86	1.47
PPC-1	2.67	0.89	1.33
PPC-2	2.53	0.91	1.34

Crystallization kinetics

In this study, crystallization kinetic is discussed with Jeziorny approach.[33] The Avrami equation[34] is involved as well. For comparison, the crystallization kinetics of PP is also discussed.

$$1 - X_t = \exp(-Z_t t^n) \quad (1)$$

Equation (1) is the Avrami equation, where Z_t is the growth rate constant and n is the Avrami exponent representing the nucleation mechanism and growth dimension of crystallization. The relative degree of crystallinity of X_t, as a function of crystallization time t, can be formulated as

$$X_t = X_c(t)/X_c(t_\infty) = \int_0^t \left(\frac{dH_t}{dt}\right)dt \Big/ \int_0^\infty \left(\frac{dH_t}{dt}\right)dt$$

Figure 6 shows X_t as a function of t for PP and its nanocomposites. The half-time of crystallization $t_{1/2}$ could be estimated from Figure 6 for PP and its nanocomposites, and the results are listed in Table III. On the basis of eq. (1), plotting ln[−ln (1−X_t)] against ln(t) straight lines should be obtained as shown in Figure 7. Then, the values of ln(Z_t) and n for PP and its nanocomposites could be estimated from the intercept and slope of the plot, respectively. On the basis of Jeziorny

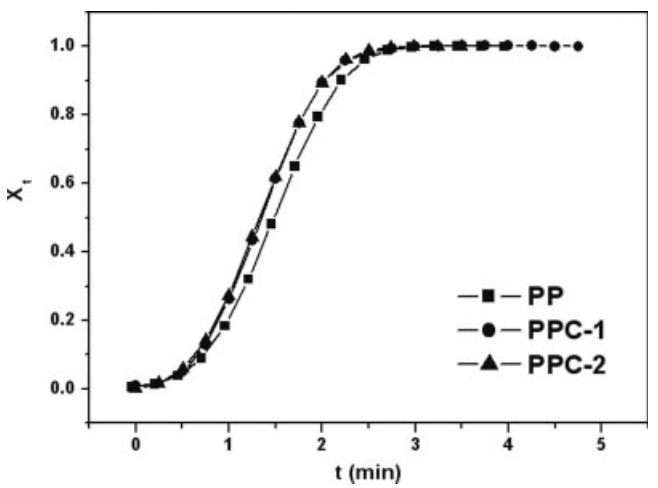

Figure 6 Plots of X_t versus t for crystallization of PP and PP/$CaCO_3$ nanocomposites.

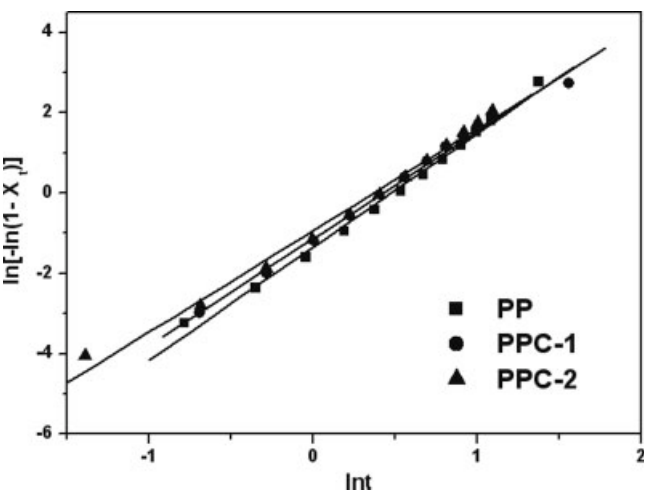

Figure 7 Plots of ln[−ln (1−X_t)] versus ln$t$ for crystallization of PP and PP/$CaCO_3$ nanocomposites.

approach, the value of $\ln(Z_t)$ could be calculated by the following formulation

$$\ln(Z_c) = \ln(Z_t)/R \quad (2)$$

where Z_c is the modified growth rate constant, and R is the cooling rate. Values of n and Z_c are also summarized in Table III.

Comparing with pure PP, it can be seen that the values of Z_c increase and the values of $t_{1/2}$ reduce somewhat for the two PP/$CaCO_3$ nanocomposites, which means that the rate of crystallization for PP/$CaCO_3$ nanocomposites is faster than for pure PP. This is due to the heterogeneous nucleation of $CaCO_3$ nanoparticles, just as the reason for the change of crystallization temperature mentioned in the previous section.

From Table III, it can be found that there are no significant differences in the related kinetics parameters for PPC-1 and PPC-2. This is because the $CaCO_3$ nanoparticles have different effects at different stages of crystallization process. On one hand, the coupling agent could improve the compatibility between nanoparticles and PP matrix and facilitate heterogeneous nucleation step; on the other hand, strong interfacial interaction between $CaCO_3$ nanoparticles and the polymer could hinder the motion of macromolecular chains to some extent during crystal growing step. As a result, there is a petty difference in the total rate of crystallization for PPC-1 and PPC-2.

Crystallization morphology of nanocomposites

Figure 8 shows the POM micrographs of pure PP (a), PPC-1 (b), and PPC-2 (c). Although pure PP displays the common spherulites with sharp and clear birefringence, there exists difference in spherulitic structure for PPC-1 and PPC-2. Usually, the number of nucleation sites determines the morphology of growing crystallites because a large number of nucleation centers would lead to a large number of small crystallites. Obviously, in Figure 8, it can be seen that the spherulites of the nanocomposites become smaller than that of pure PP and are distorted and interlaced with one another. This is due to nucleating effects of nanofillers. In addition, compared with PPC-1, the spherulite size of PPC-2 is much smaller than that of PPC-1. When CA-2 is used to modify the $CaCO_3$ nanoparticles, much stronger interfacial interaction may form in PPC-2 (that is also mentioned in other sections of this paper), which results in an enhanced dispersion and nucleation effect for nanopaticles. Therefore, more nucleation sites would form in PPC-2, and the spherulite size of PPC-2 would become smaller.

Formation of β-phase crystal

The samples directly cut from the molded sheet are heated from room temperature to 180°C at the rate of 5°C/min. The melting curves are shown in Figure 9. Figure 10 displays the X-ray diffraction patterns for these samples. It is obviously seen in Figure 9 that two melting peaks (In Fig. 9, T_{m1} and T_{m2} represent the low temperature peak and the high temperature peak, respectively.) appear for PP/$CaCO_3$ nanocomposites and only one melting peak appears for pure PP. The melting temperatures (T_{m1} and T_{m2}) for PPC-1 and PPC-2 are both about 151 and 169°C, respectively. It is already known that PP can form α-phase crystal at relative higher crystallization temperature and β-phase crystal at relative lower crystallization temperature. This phenomenon is also observed in our experiment.

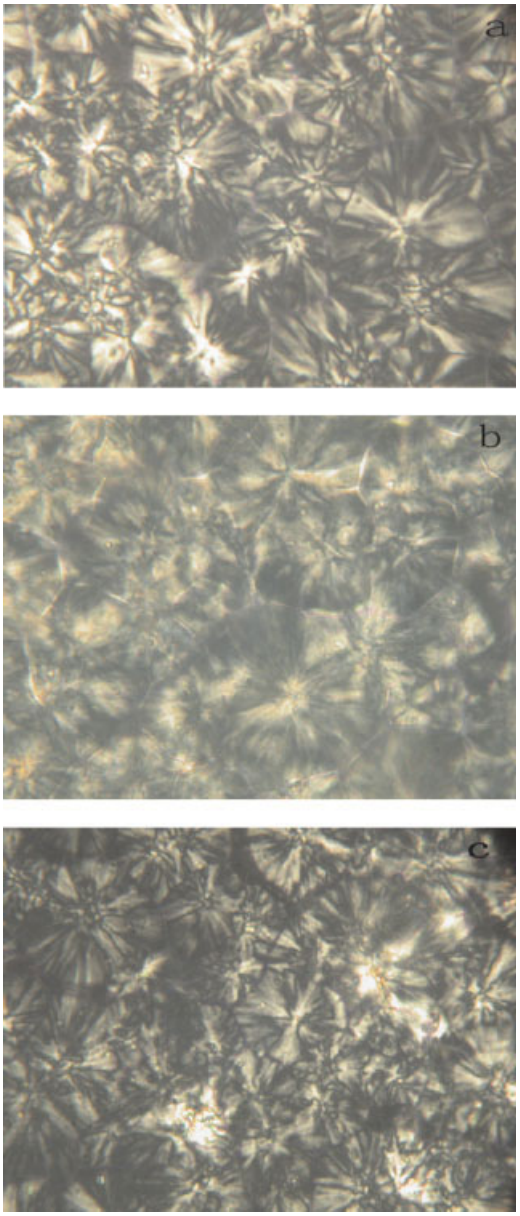

Figure 8 POM micrographs of pure PP (a), PPC-1 (b), and PPC-2 (c) with magnification of 400. [Color figure can be viewed in the online issue, which is available at www.interscience.wiley.com.]

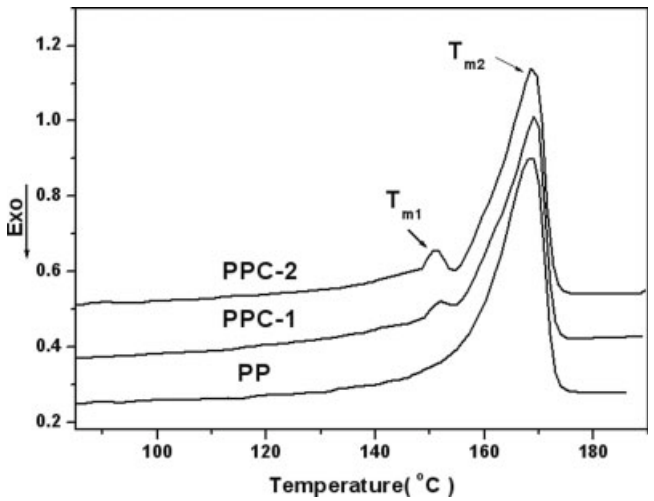

Figure 9 DSC heating curves of PP and PP/$CaCO_3$ nanocomposites at the rate of 5°C/min.

Both CA-2 and CA-1 modified $CaCO_3$ nanoparticles can induce the formation of β-phase crystal. The peak area of β-phase crystal for PPC-2, however, is somewhat bigger than that of PPC-1. And the shape of low temperature peak of PPC-2 is also sharper than that of PPC-1.

The results of X-ray diffraction patterns of PP and PP/$CaCO_3$ nanocomposites give more information about β-phase crystal in Figure 10. Besides that PPC-1 and PPC-2 have the same [(110), (040), (130), (111), and (131)] faces of α-phase crystal as pure PP had, they also have the (300) face of β-phase crystal. On the basis of the intensity of the (300) face peak, the relative amount of β-phase crystal can be calculated by the following equation[35]

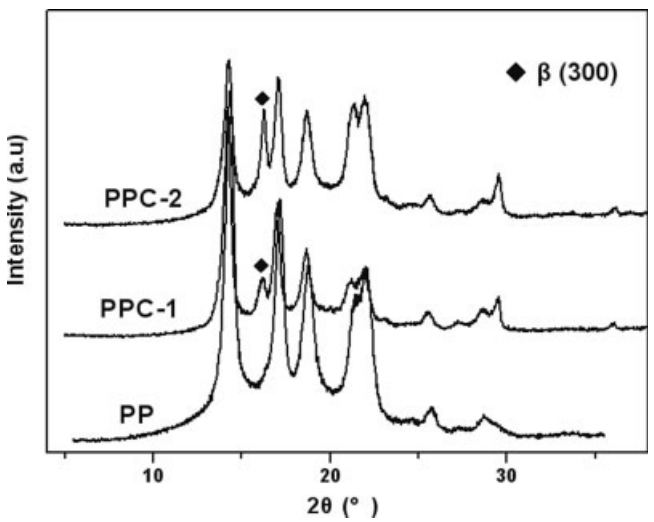

Figure 10 X-ray diffraction patterns for PP and PP/$CaCO_3$ nanocomposites.

$$K = \frac{H_{(300)}}{H_{(110)} + H_{(040)} + H_{(130)} + H_{(300)}} \times 100\%$$

where $H_{(100)}$, $H_{(040)}$, and $H_{(130)}$ are the values of the three most intensities for α-phase crystal, and $H_{(300)}$ is for β-phase crystal. The relative amounts of β-phase crystal for PPC-1 and PPC-2 are 17.55 and 40.67%, respectively. The relative amount of β-phase crystal for

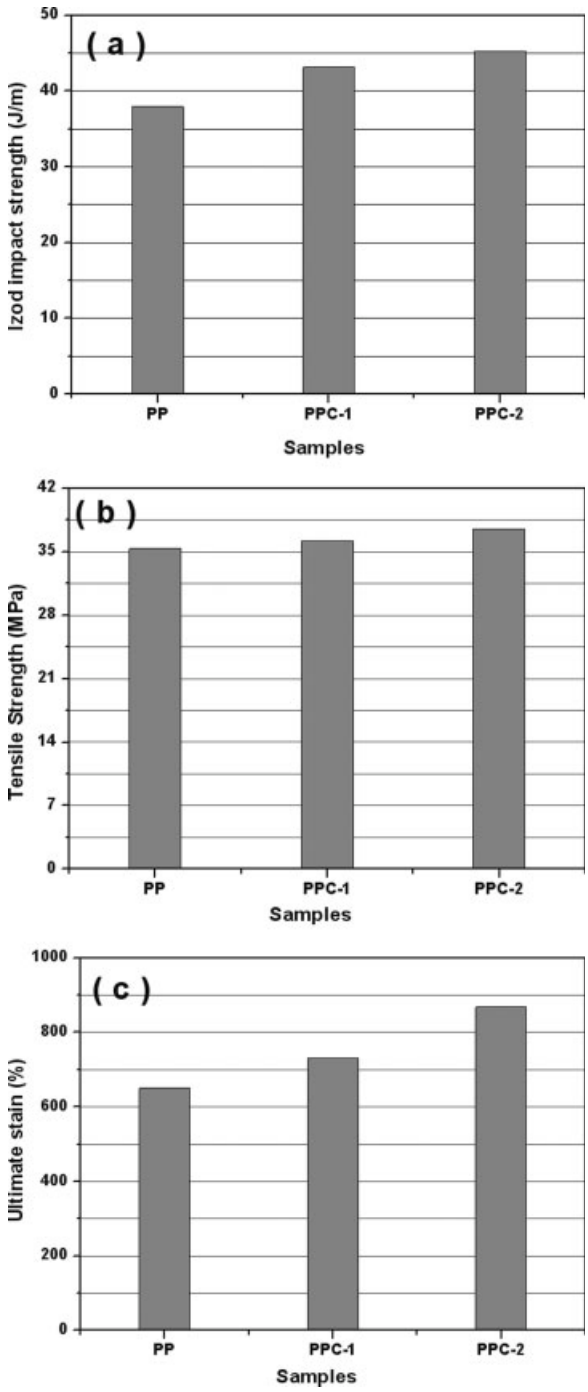

Figure 11 The mechanical properties of PP and PP/$CaCO_3$ nanocomposites: (a) Impact strength; (b) Tensile strength; (c) Ultimate strain.

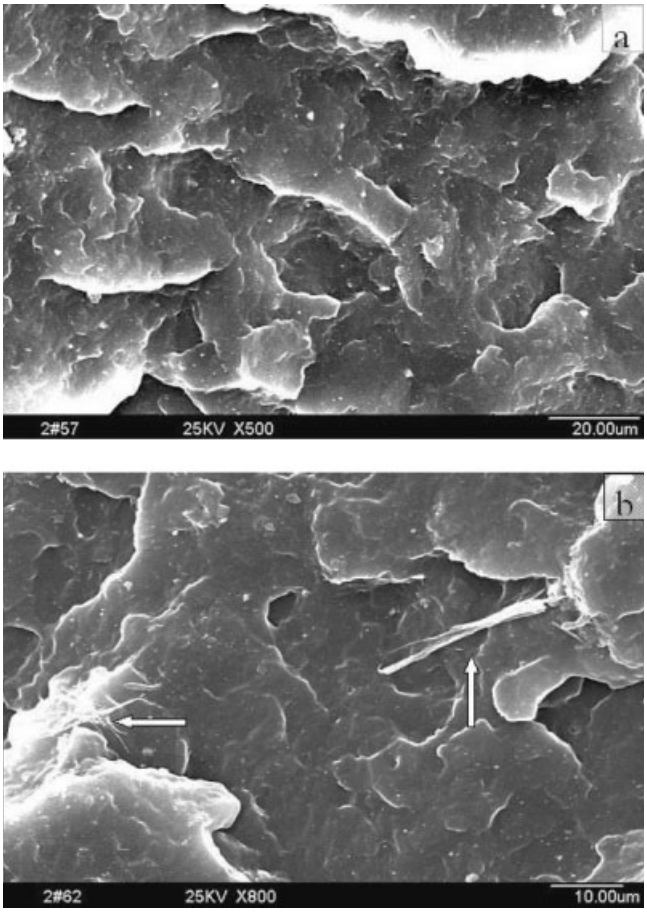

Figure 12 SEM micrographs of impact-fractured surface of PPC-1 viewed under low (a) and high (b) magnifications.

PPC-2 is up to 20% higher than that for PPC-1. Apparently, the ability of CA-2 modified $CaCO_3$ nanoparticles on inducing β-phase crystal is much stronger than that of CA-1 modified nanoparticles. It is known that the formation of β-phase crystal is mainly related to process conditions and component of materials. Compared with CA-1, CA-2 is a compound surface-treating agent consisting of aluminate coupling agent and stearic acid compatilizer. The existence of stearic acid compatilizer may cause a synergistic effect and result in a stronger interfacial interaction, which induces much more β-phase crystal in PPC-2.

Mechanical properties

The mechanical properties of pure PP and PP/$CaCO_3$ nanocomposites are shown in Figure 11(a–c). Compared with pure PP, the mechanical properties of PP/$CaCO_3$ nanocomposites were all improved. The impact strength, the tensile strength, and the ultimate strain of PPC-2 were increased by approximately 16.5, 4.3, and 23.0%, respectively, which means that adding $CaCO_3$ nanoparticles is an effective way to strengthen and toughen the PP matrix. As shown in Figure 11, the impact strength, the tensile strength and the ultimate strain of PPC-2 were approximately 4.9, 3.7, and 18.5% higher than that of PPC-1, respectively. Obviously, CA-2 modified $CaCO_3$ nanoparticles can improve the toughness of PP/$CaCO_3$ nanocomposites more effectively. Figure 12 and Figure 13 give more information about it.

Figure 12 shows SEM micrographs of the impact-fractured surface of PPC-1. Although the nanoparticles under the size of 100 nm disperse uniformly in PP matrix, the microstructure of nanocomposites presents phase separation when viewed under low magnification [Fig. 12(a)], which causes the composites to fracture easily under loads. When viewed at high magnification [Fig. 12(b)], highly stress-concentration zones are observed apparently in the fractured surface (arrows), which usually cause decrease in toughness of nanocomposites.

Figure 13 shows SEM micrographs of the impact-fractured surface of PPC-2. Compared with Figure 12(a), there is nearly no $CaCO_3$ nanoparticles exposing in the fractured surface as observed in Figure 13(a), and no significant stress-concentration zones are

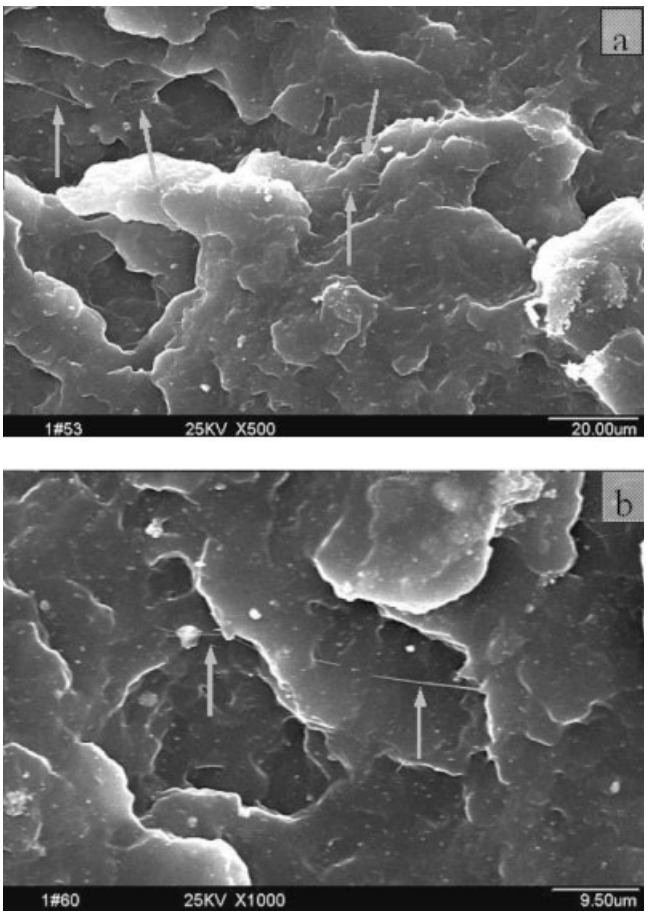

Figure 13 SEM micrographs of impact-fractured surface of PPC-2 viewed under low (a) and high (b) magnification.

viewed under high magnification [Fig. 13(b)]. Moreover, an interesting microphenomenon, named as ''drawing silk,'' is shown in Figure 13 (arrows). This indicates that the interfacial interaction between nanoparticles and PP in PPC-2 are stronger than that in PPC-1, which results in a better toughness in PPC-2. This is in accordance with the results of preceding section.

Actually, the improved toughness of the PP-based nanocomposites is directly related to the small size of spherulites and the formation of β-phase crystal. The small size of spherulites is favorable to absorb the impact energy of loadings. The β-phase crystal of PP has also been long recognized to have a greater mechanical absorption capacity than α-phase crystal. Therefore, the major reason for the improved impact property and enhanced toughness of PPC-2 is that there exist much smaller spherulites and β-phase crystal than that of PPC-1.

CONCLUSIONS

PP/$CaCO_3$ nanocomposites (PPC-1 and PPC-2), with CA-1 modified and CA-2 modified $CaCO_3$ nanoparticles, respectively, were prepared by melt blending. The TEM study showed that the CA-2 modified nanoparticles dispersed much better than the CA-1 modified nanoparticles in PP matrix. The DSC study showed that the onset crystallization temperature of PPC-2 was about 3°C lower than that of PPC-1. In addition, the $CaCO_3$ nanoparticles affected the crystallization process in two opposite ways: facilitate the nucleating process and impede the crystal growth process. Therefore, there were no significant differences in the total rate of crystallization for PPC-1 and PPC-2. POM observation exhibited much smaller spherulites in PPC-2 than PPC-1 and pure PP. Results of mechanical properties indicated that the toughness of PPC-2 was much better than that of PPC-1. The XRD analysis revealed that CA-2 modified $CaCO_3$ nanoparticles could induce more β-phase crystal by approximately 20% than CA-1 modified $CaCO_3$ nanoparticles could, which may be caused by a synergistic effect of aluminate coupling agent with stearic acid. Above all, diminished spherulitic morphology and β-phase crystal contributed to the improved mechanical properties.

References

1. Paunikallio, T.; Kasanen, J.; Suvanto, M.; Pakkanen, T. T. J Appl Polym Sci 2003, 87, 1895.
2. García Martínez, J. M.; Laguna, S.; Areso, S.; Collar, E. P. J Polym Sci Part B: Polym Phys 2000, 38, 1564.
3. Tjong, S. C.; Meng, Y. Z. J Polym Sci Part B: Polym Phys 2003, 41, 2332.
4. Chow, W. S.; Mohd Ishak, Z. A.; Ishiaku, U. S.; Kocsis, J. K.; Apostolov, A. A. J Appl Polym Sci 2004, 91, 175.
5. Tidjani, A. Polym Degrad Stab 2005, 87, 43.
6. Grozdanov, A.; Buzarovska, A.; Gaceva, G. B.; Nedkov, E. J Polym Sci Part B: Polym Phys 2005, 43, 66.
7. Saujanya, C.; Radhakrishnan, S. Polymer 2001, 42, 6723.
8. Zheng, J. R.; Siegel, R. W.; Toney, G. J Polym Sci Part B: Polym Phys 2003, 41, 1033.
9. Pavliková, S.; Thomann, R.; Reichert, P.; Mülhaupt, R. J Appl Polym Sci 2003, 89, 604.
10. Li, J.; Zhou, C. X.; Wang, G.; Zhao, D. L. J Appl Polym Sci 2003, 89, 3609.
11. Xu, N.; Zhou, W.; Shi, W. F. Polym Adv Technol 2004, 15, 654.
12. Chen, L.; Wong, S. C.; Liu, T. X.; Lu, X. H.; He, C. B. J Polym Sci Part B: Polym Phys 2004, 42, 2759.
13. Zhang, Y. Q.; Lee, J. H.; Jang, H. J.; Nah, C. W. Compos B 2004, 35, 133.
14. Koo, C. M.; Kim, J. H.; Wang, K. H.; Chung, I. J. J Polym Sci Part B: Polym Phys 2005, 43, 158.
15. Chiu, F. C.; Lai, S. M.; Chen, J. W.; Chu, P. H. J Polym Sci Part B: Polym Phys 2004, 42, 4139.
16. Hambir, S.; Bulakh, N.; Kodgire, P.; Kalgaonkar, R.; Jog, J. P. J Polym Sci Part B: Polym Phys 2001, 39, 446.
17. Wang, Y.; Chen, F. B.; Wu, K. C. J Appl Polym Sci 2004, 93, 100.
18. Thio, Y. S.; Argon, A. S.; Cohen, R. E.; Weinberg, M. Polymer 2002, 43, 3661.
19. Gaymans, W. C. J.; Westzaan, C.; Huetink, J.; Gaymans, R. J. Polymer 2003, 44, 261.
20. Argon, A. S.; Cohen, R. E. Polymer 2003, 44, 6014.
21. Ren, Z.; Shanks, R. A.; Rook, T. J. J Appl Polym Sci 2001, 79, 1942.
22. Chan, C. M.; Wu, J. S.; Li, J. X.; Cheung, Y. K. Polymer 2002, 43, 2981.
23. Ansari, D. M.; Price, G. J. J Appl Polym Sci 2003, 88, 1951.
24. Zhang, Q. X.; Yu, Z. Z.; Xie, X. L.; Mai, Y. W. Polymer 2004, 45, 5985.
25. Zhu, W. P.; Zhang, G. P.; Yu, J. Y.; Dai, G. J Appl Polym Sci 2004, 91, 431.
26. Labour, T.; Vigier, G.; Séguéla, R.; Gauthier, C.; Orange, G.; Bomal, Y. J Polym Sci Part B: Polym Phys 2002, 40, 31.
27. Lin, Z. D.; Huang, Z. Z.; Zhang, Y.; Mai, K. C.; Zeng, H. M. J Appl Polym Sci 2004, 91, 2443.
28. Mittal, K. L. Silanes and Other Coupling Agents; VSP: The Netherlands, 1992.
29. Shi, G. Y.; Zhang, J. Y.; Jin, H. S. Chin. Pat. CN 85 100 465A (1985).
30. Liao, K. R.; Chen, X. X.; Zheng, C. R. Chem J Chin Univ 1995, 16, 143.
31. Feng, J. C.; Chen, M. C.; Huang, Z. T. Chem J Chin Univ 2001, 22, 154.
32. Turi, E. A. Thermal Characterization of Polymeric Materials; Academic Press: New York, 1981.
33. Jeziorny, A. Polymer 1978, 19, 1142.
34. Avrami, M. J. Chem Phys 1940, 8, 212.
35. Yin, J. H.; Mo, Z. S. Modern Physics of Polymer; Science Press: Beijing, 2001.